**Supplementary Material for:**

**Kruiver et al. (2022) Capturing spatial variability in the regional Ground Motion Model of Groningen, the Netherlands,** *Netherlands Journal of Geosciences*

This Supplementary Material contains extra figures supporting the analysis of the ambient noise $V_{S\_to\_100m}$ field data (Figures S1-S2), differences in velocity structure between model and field data (Figures S3-S4) and histograms supporting our choice for analysing amplification factors *AF* instead of ln(*AF*) (Figures S5-S8).

The beamforming technique (Rost & Thomas, 2002; Boué et al., 2013) shows the orientation of noise sources through coherent seismic energy. The continuous seismic data are the input for the beamforming analysis, which is performed in different frequency bands. The beamforming results are displayed in Figure S1. The results show that the noise direction is fairly isotropic among the different frequency bands and that the highest energy comes from the west to north quadrant. This agrees well with the general direction of the North Sea, which acts as the main source of ambient noise.
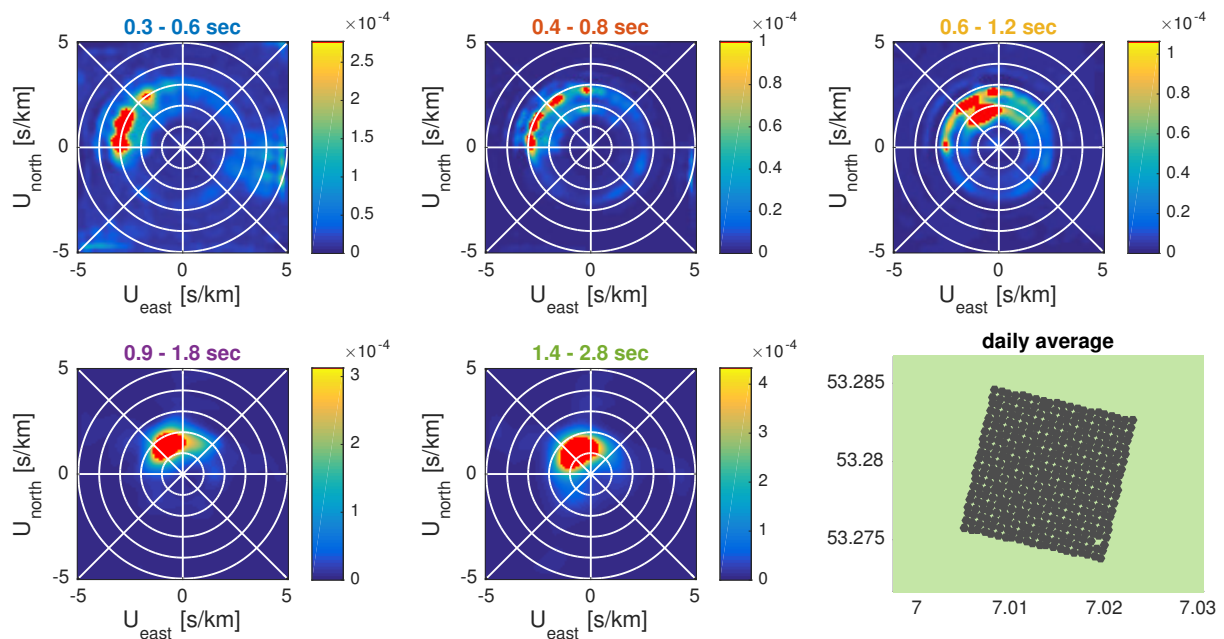


*Figure S1. Beamforming analysis results for Borgsweer for the ambient noise data field data with target depth of 100 m, averaged over the whole acquisition period, in 5 different frequency bands.*

Figure S2 shows the azimuthal distribution of dispersion curves used in surface wave tomography that remain after the quality check of dispersion curves. The South-West/North-East directions are dominating for all periods, due to the orientation of the main noise sources and the line of receivers. The period bands shown in Figure S1 and Figure S2 are different, because the beamforming is the first step of an exploratory process to understand noise sources and the azimuthal distribution depends on the frequency bands that provided good quality data for picking of the dispersion curves.
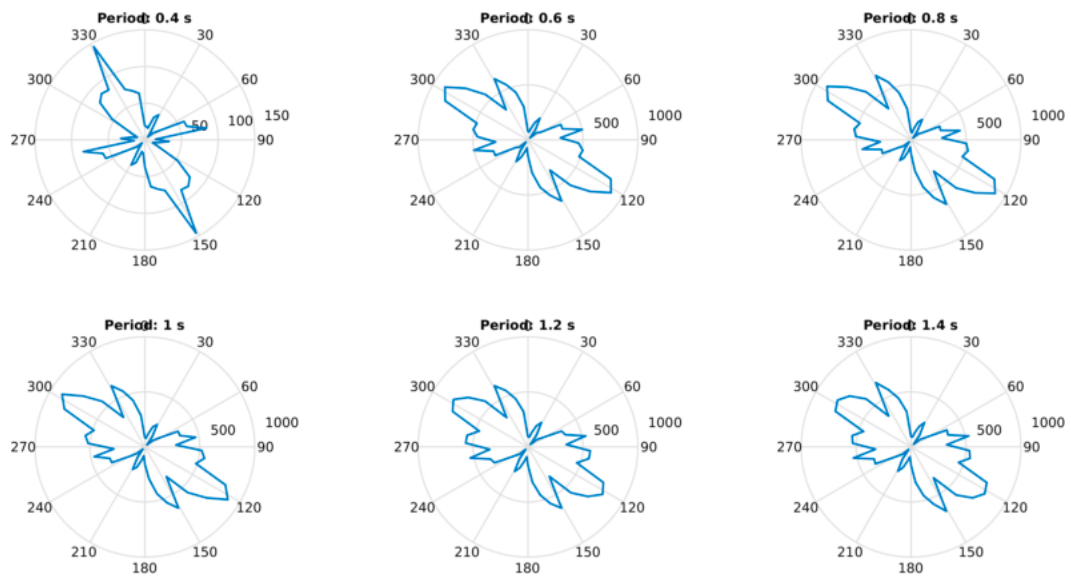
*Figure S2. Azimuthal distribution of the Rayleigh wave paths used for the tomography at each period. The number to the right indicates the number of dispersion curves.*

The difference in $V_S$ between the field data and the model data has been visualised in Figure S3 for Borgsweer and Figure S4 for Loppersum. For all coordinates within each $V_{S\text{-}to\text{-}100m}$ block, the difference between the model $V_S$ and the field $V_S$ (model-field) has been averaged over bins of 5 m thickness. The mean and standard deviation per bin is plotted. These figures show that - on average - the field $V_S$ is lower than the model $V_S$ in the top 100 m.
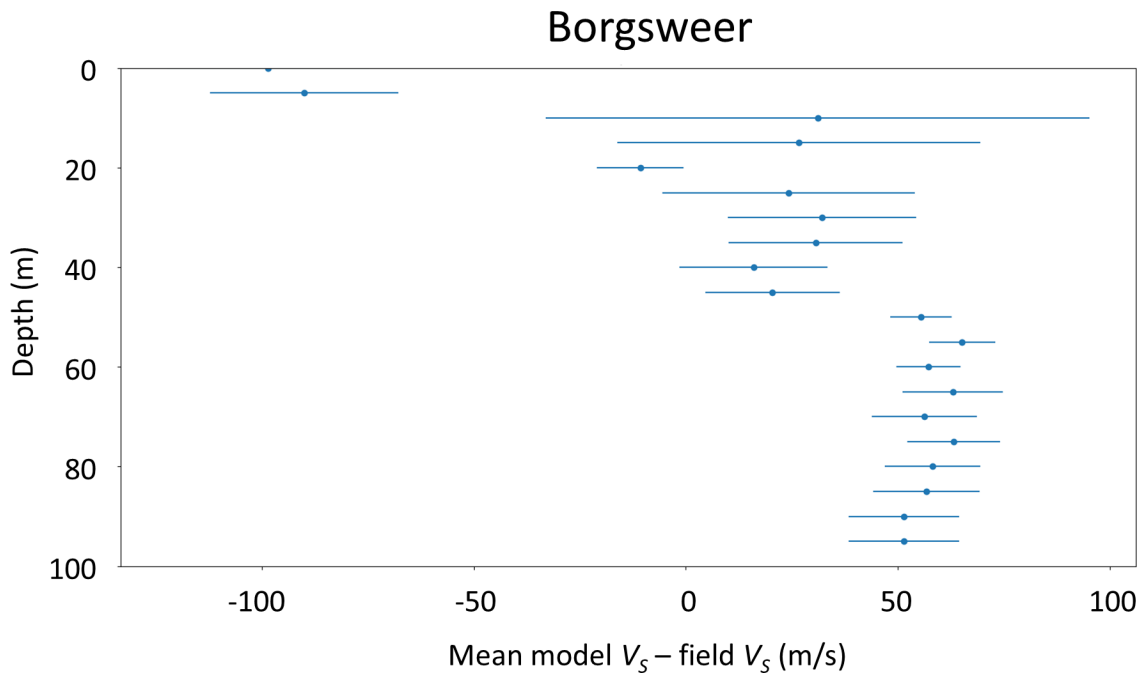


*Figure S3. Borgsweer: Mean difference (dot) and standard deviation (horizontal line) in $V_S$ between the model $V_S$ and the field $V_S$ (model minus field), averaged over all coordinates in the $V_{S\text{-}to\text{-}100m}$ block.*
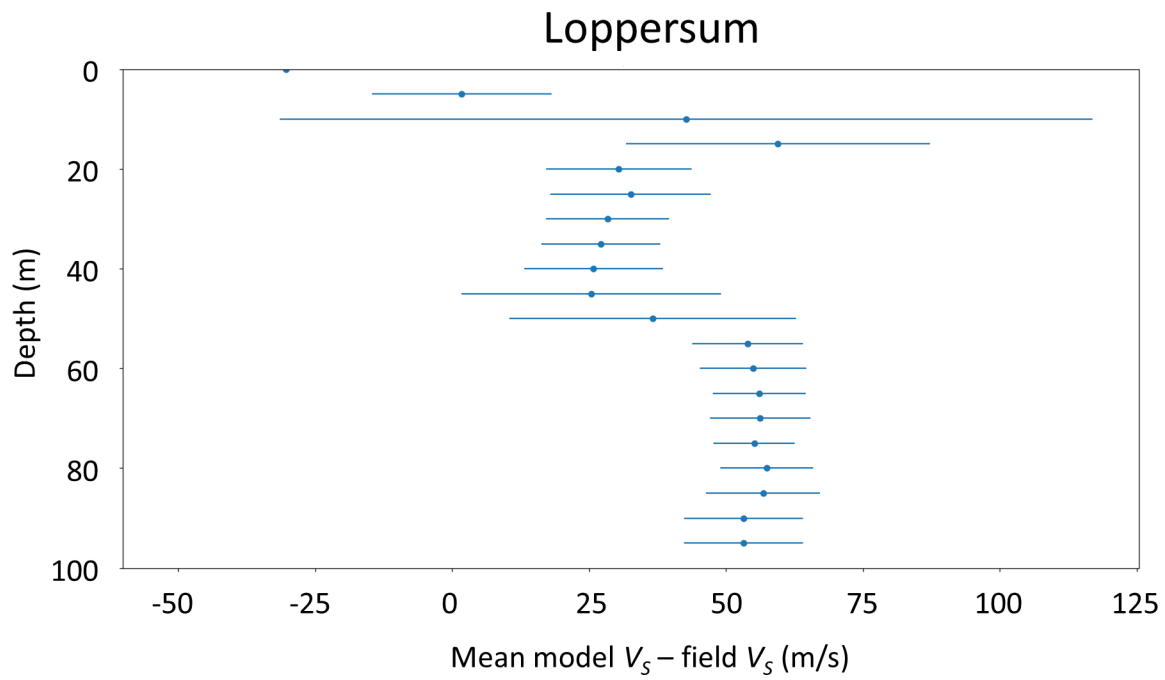
*Figure S4. Loppersum: Mean difference (dot) and standard deviation (horizontal line) in $V_S$ between the model $V_S$ and the field $V_S$ (model minus field), averaged over all coordinates in the $V_{S\text{-to-}100m}$ block.*

The *AF* results distributions were analysed and shown as histograms for all 23 periods in Figures S5-S8. For some periods, the distribution appears to be normal, for other periods log-normal and for other periods neither normal nor log-normal. Statistical tests were inconclusive for either normally or log-normally distributed data. Therefore, the *AF* results were analysed in linear space and not converted to natural logarithms of *AF*.
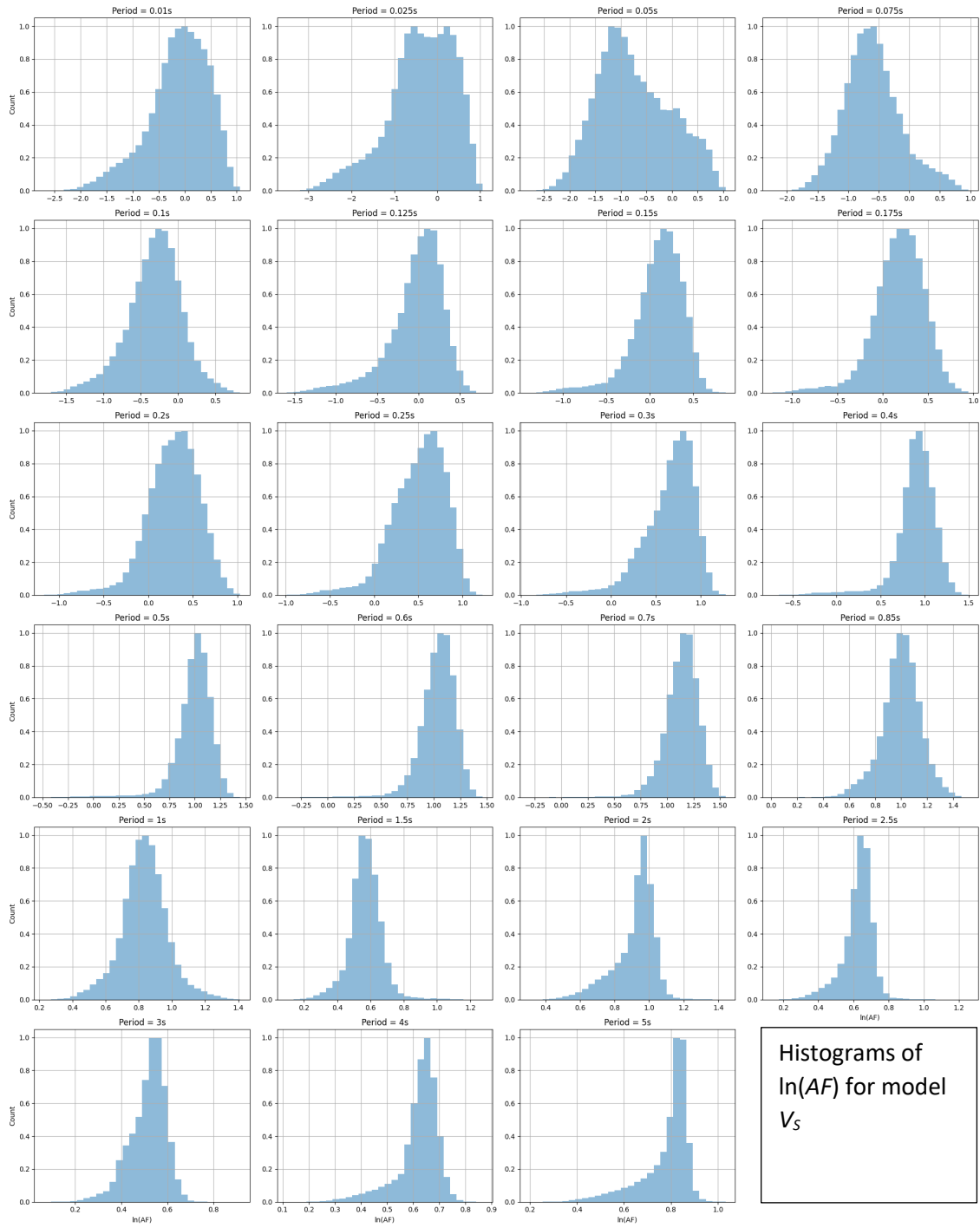
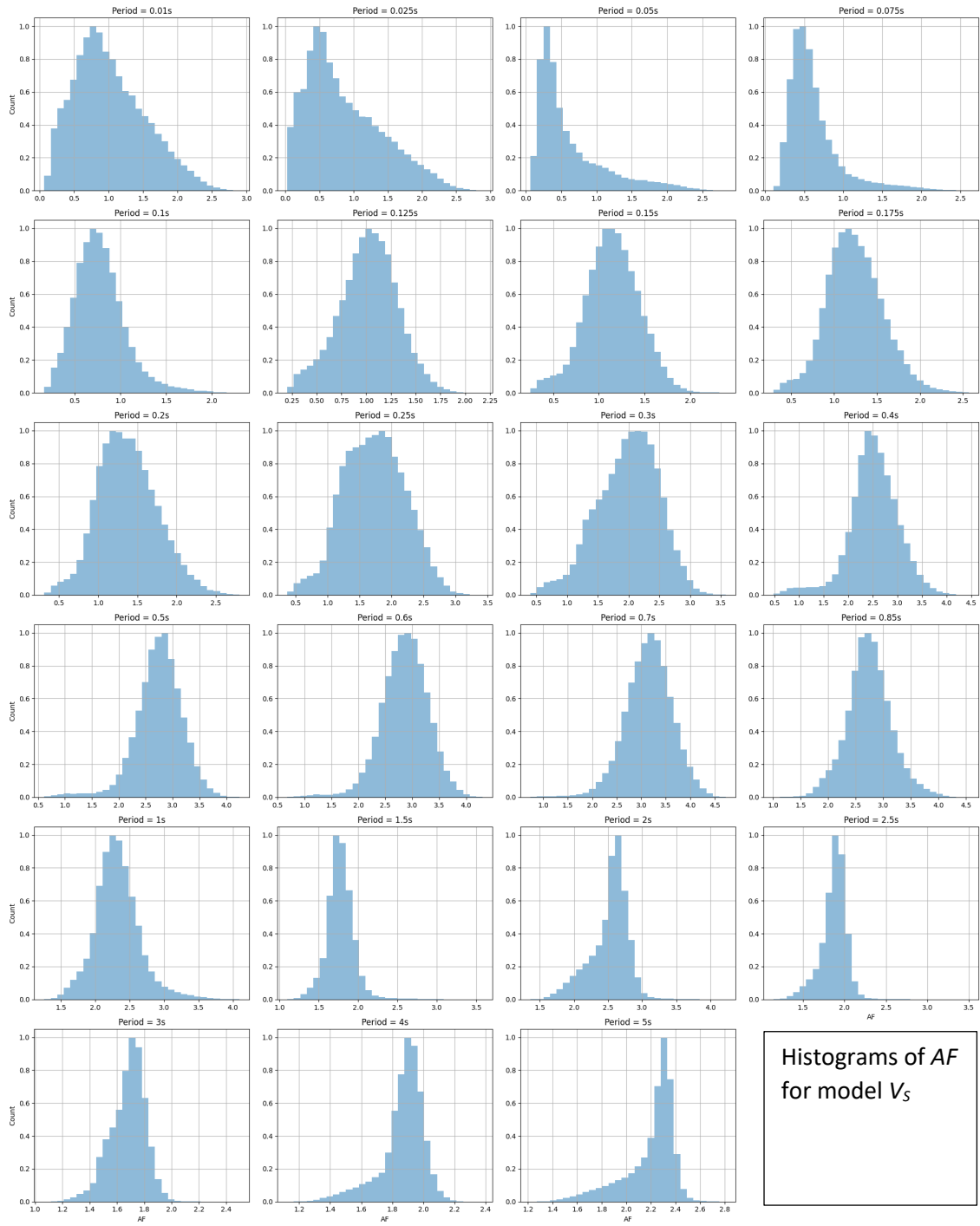*Figure S5. Histograms of ln(AF) for model VS (option A).*

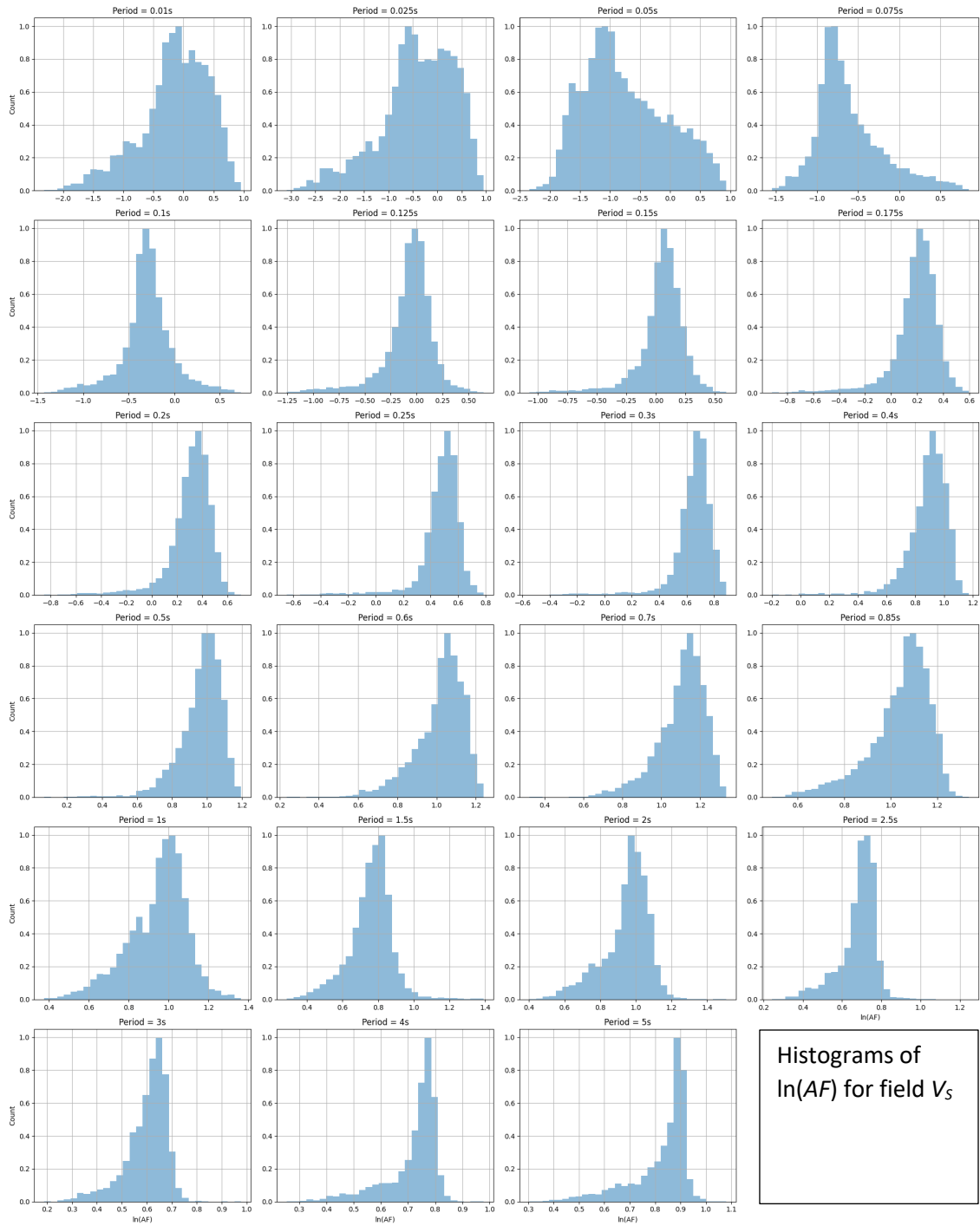*Figure S6. Histograms of AF for model $V_S$ (option A).*

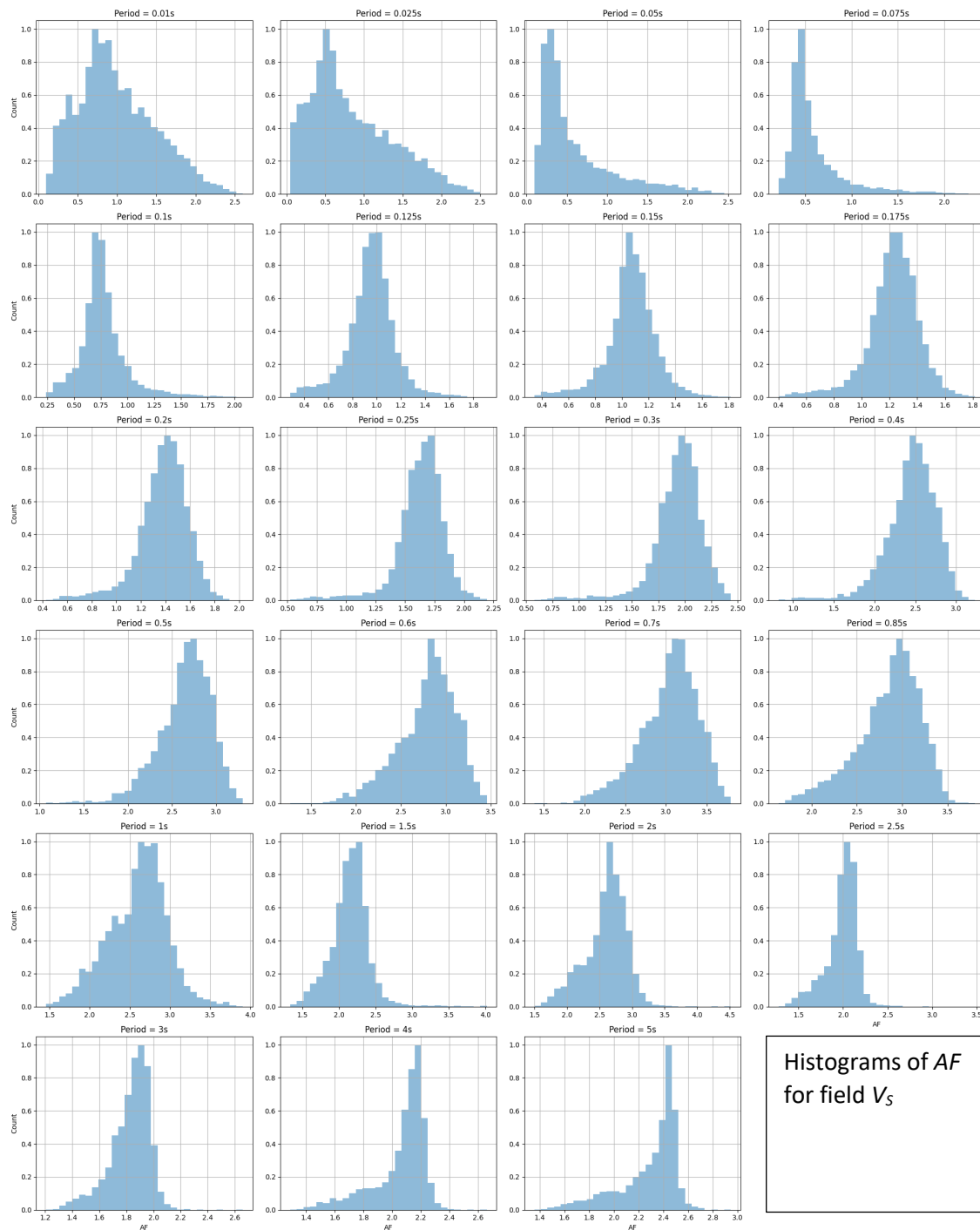*Figure S7. Histograms of ln(AF) for field V$_S$ (option B).*

*Figure S8. Histograms of AF for field V_S (option B).*

**References:**

Boué, P., Roux, P., Campillo, M. & de Cacqueray, B., 2013. Double beamforming processing in a seismic prospecting context. Geophysics, 78: V101-V108. https://doi.org/10.1190/geo2012-0364.1

Rost, S., & Thomas, C., 2002. Array seismology: Methods and applications. Reviews of geophysics, 40(3), 2-1. https://doi.org/10.1029/2000RG000100